International Journal of Chemical, Materials and Biomolecular Sciences
ISSN: 2415-6620
Vol:7, No:12, 2013

Effect of Rotation Rate on Chemical Segragation during Phase Change

Nouri Sabrina, Benzeghiba Mohamed, Ghezal Abderrahmane

***Abstract*—**Numerical parametric study is conducted to study the effects of ampoule rotation on the flows and the dopant segregation in vertical bridgman (vb) crystal growth. Calculations were performed in unsteady state. The extended darcy model, which includes the time derivative and coriolis terms, has been employed in the momentum equation. It's found that the convection, and dopant segregation can be affected significantly by ampoule rotation, and the effect is similar to that by an axial magnetic field. Ampoule rotation decreases the intensity of convection and stretches the flow cell axially. When the convection is weak, the flow can be suppressed almost completely by moderate ampoule rotation and the dopant segregation becomes diffusion-controlled. For stronger convection, the elongated flow cell by ampoule rotation may bring dopant mixing into the bulk melt reducing axial segregation at the early stage of the growth. However, if the cellular flow cannot be suppressed completely, ampoule rotation may induce larger radial segregation due to poor mixing.

***Keywords*—**Numerical Simulation-Heat and mass transfer-vertical solidification-chemical segregation.

I. Introduction

THE control of melt flow is important in crystal growth. Besides eliminating unstable flows that causes growth striations it also affects dopant segregation [1]-[3]. However, the heat flow and chemical segregation in the process strongly depend on ampoule orientation and heating uniformity. To minimize the unstable flow and convection, the ampoule is usually aligned with the gravity orientation and the melt sits upon the growth interface, this the so-called vertical Bridgman (VB) configuration. However, perfect alignment and uniform heating are hard to obtain in practice. To improve the quality of the product obtained, we need to damp the buoyancy convection sufficiently to reach the diffusion-controlled limit [4]. The most well known approach is the use of magnetic damping [5]-[7]. The flow intensity $(\psi_{\max})$ decreases with the increasing magnetic field strength (B or in terms of Hartmann number Ha); $\psi_{\max} \sim Ha^{-2}$ [8], [9]. However, the hardware requirement to provide a sufficient magnetic damping (usually in the order of 0.5T) is expensive. An alternative way to suppress the flow may be other mechanisms like vibration [10]-[12] as well is the use of steady ampoule rotation. As discussed by [13], [14], a moderate rotation rate may affect the buoyancy flow significantly for the axisymmetric configuration. In addition, its damping effect is similar to that due to the magnetic field but less effective; $\psi_{\max} \sim \Omega^{-1}$ [15], where Ω is the rotation speed.

In the present study, an axisymmetric numerical simulation is conducted to investigate the effects of ampoule rotation on axisymmetric fluid flow and segregation under perfect growth conditions. To further illustrate the feasibility of using ampoule rotation for flow damping, different rotation rates whose represented by the Reynolds numbers are considered and the reduce of buoyancy convection situations, represented by the Rayleigh number, and chemical radial segregations are discussed. In the next section, the model and its numerical simulation are briefly described. Section III is devoted to the results and discussion. Finally; we tried to summarize the main physical conclusions of this study.

II. Model Description and Mathematical Formulation

The schematic of the VB crystal growth used in this study is depicted in Fig. 1. The furnace is described by an effective heating profile $T_a(z,t)$, which is assumed linear in this study. For unsteady state calculations, the thermal profile is varying with time and the ampoule is moved downward at a speed V_g.

$$T_a(z,t) = -\frac{(T_h - T_c)}{L_g} V_g t \times T_h \tag{1}$$

where T_h and T_c are respectively the temperatures of the hot and cold zones. L_g is the length of the temperature profile zone.

Dr. Nouri Sabrina is with Science and Technology university Houri Boumedienne 16000 Algeriers, Algeria (phone: +213-661-295-203; e-mail: nouri290676@yahoo.fr).

Dr. Benzeghiba Mohamed is with the Ifp Drilling and Completion Dept, Pau, France (e-mail: m_benzeghiba@yahoo.fr).

Dr. Ghezal Abderrahmane is with Science and Technology University Houri Boumedienne 16000 Algeriers, Algeria (e-mail: aghezal@yahoo.fr).

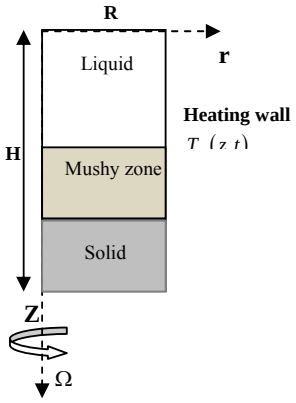

Fig. 1 Schematic of vertical Bridgman Growth (VG)

The system is assumed to be axisymmetric and the initial dopant distribution in the melt is assumed uniform at C_0. The flow and solute distribution are represented in a cylindrical coordinate system (r,z). The melt is assumed incompressible and Newtonian, while the flow is laminar. The Boussinesq approximation is also adopted for buoyancy forces. The stream function ψ is defined in terms of radial (u) and axial (v) velocities as

$$u = -\frac{\partial \psi}{r\partial z}, \quad v = \frac{\partial \psi}{r\partial r} \tag{2}$$

The unsteady-state governing equations for velocity field (u,v), temperature (T) and dopant concentration (C) in the conservative-law can be expressed by:

Continuity Equation

$$\frac{1}{r}\frac{\partial(ru)}{\partial r} + \frac{\partial v}{\partial z} = 0 \tag{3}$$

Momentum Equation

$$\frac{\partial u}{\partial t} + u\frac{\partial u}{\partial r} + v\frac{\partial u}{\partial z} - \left(1 - \frac{Gr}{\mathrm{Re}^2}\left((T-1) + N(C-1)\right)\right)\frac{w^2}{r} = -\frac{\partial p}{\partial r} + \frac{1}{\mathrm{Re}}\left(\frac{1}{r}\frac{\partial}{\partial r}\left(r\frac{\partial u}{\partial r}\right) + \frac{\partial}{\partial z}\left(\frac{\partial u}{\partial z}\right) - \frac{u}{r^2}\right) - \frac{\eta\varepsilon}{\mathrm{Re}}u \tag{4}$$

$$\left(\frac{\partial v}{\partial t} + u\frac{\partial v}{\partial r} + v\frac{\partial v}{\partial z}\right) = -\frac{\partial p}{\partial z} + \frac{1}{\mathrm{Re}}\left(\frac{1}{r}\frac{\partial}{\partial r}\left(r\frac{\partial v}{\partial r}\right) + \frac{\partial}{\partial z}\left(\frac{\partial v}{\partial z}\right)\right) - \frac{\varepsilon}{\mathrm{Re}}v + \left(1 - \frac{Gr}{\mathrm{Re}^2}\left((T-1) + N(C-1)\right)\right) \tag{5}$$

$$\left[\frac{\partial w}{\partial t} + v\frac{\partial w}{\partial z} + u\frac{\partial w}{\partial r}\right] + \left(1 - \frac{Gr}{\mathrm{Re}^2}\left((T-1) + N(C-1)\right)\right)\frac{v.w}{r} = \frac{1}{\mathrm{Re}}\left[\frac{\partial}{r\partial r}\left(r\frac{\partial w}{\partial r}\right) - \frac{w}{r^2} + \frac{\partial^2 w}{\partial z^2}\right] - \frac{\varepsilon}{\mathrm{Re}}w \tag{6}$$

Energy Equation

$$\left(\frac{\partial T}{\partial t} + u\frac{\partial T}{\partial r} + v\frac{\partial T}{\partial z}\right) = \frac{1}{\mathrm{Pr}\,\mathrm{Re}}\left(\frac{1}{r}\frac{\partial}{\partial r}\left(r\frac{\partial T}{\partial r}\right) + \frac{\partial}{\partial z}\left(\frac{\partial T}{\partial z}\right)\right) + \frac{1}{Ste}\left[\frac{\partial f_s}{\partial t}\right] \tag{7}$$

Dopant Equation

$$\left((1 - f_s)\frac{\partial C}{\partial t} + u\frac{\partial C}{\partial r} + v\frac{\partial C}{\partial z}\right) = \frac{Sc}{\mathrm{Re}}\left[\frac{1}{r}\frac{\partial}{\partial r}\left(r\frac{\partial C}{\partial r}\right) + \frac{\partial}{\partial z}\left(\frac{\partial C}{\partial z}\right)\right] + (k_p - 1)C\frac{\partial(f_s)}{\partial t} \tag{8}$$

where ε is a constant ε

where p, T and C are the dimensionless pressure, temperature and dopant concentration respectively. Pr is the Prandtl number $(\mathrm{Pr} \equiv \rho C_p \nu / \lambda)$, Sc the Schmidt number $(Sc \equiv \nu / D)$. ν is the kinematic viscosity and D the dopant diffusivity in the melt. The Grashof number Gr and the buoyancy ration N in the source terms of the momentum equation are defined as follows:

$$Gr \equiv g\,\beta_T \Delta T\, R^3 / \nu^2, \quad N \equiv \beta_C \Delta C / \beta_T \Delta T$$

where g is the gravitational acceleration, $\Delta T = T_h - T_c$, β_T and β_C the thermal and solutal expansion coefficients respectively. Other, the centrifugal or rotation-driven flows are generated by the ampoule rotation. The flow pattern depen,ds on rotation rates, container radius and melts properties. The characteristic rotational Reynolds number is the ratio between inertia and viscous forces:

$$\mathrm{Re} = \Omega R^2 / \nu$$

where Ω is a characteristic rotation rate of crystal.

The Stefan number $Ste \equiv \Delta H / (C_p \Delta T)$ scales the heat fusion ΔH released during solidification to the sensible heat in the melt.

As in our previous work [16], to solve the previous equations, the solid fraction $(0 \le f_s \le 1)$ and boundary conditions need to be specified. The no-slip boundary condition for velocities is used at solid boundaries. The upper melt interface is assumed adiabatic. Compared to the nonrotating case, we need to account for an additional velocity

component, w in the azimuthally direction. The only twitch will be on the dynamic boundary conditions where $(w=0)$ on the inner's wall and $(w=1)$ on the lateral surface.

The solidification model described above has been implemented into the open source code of a 2D Navier-Stokes solver, where the SIMPLER algorithm with collocated-variables arrangement is used to calculate the pressure and the velocities. The set of equations has been discretized by a finite volume method. Time marching with fixed time step was used. The maximal number of outer iterations per time step was equal to 2000 allowing us to reach residuals of less than 10^{-3}. Detailed description of the numerical method can be found elsewhere [17].

III. Results and Discussion

The vertical crystal growth system of metallic alloy is used here to illustrate the effect of ampoule rotation on the flow and dopant segregation. The physical properties and some input parameters are listed in Tables I and in II. The mesh used here is 90×30 and further mesh refinement does not improve accuracy.

TABLE I
Experimental Input Parameters for the Vertical Bridgman System [18]

Description	Symbol	value
Crystal radius (m)	R	5×10^{-3}
Crystal length (cm)	H	70×10^{-3}
Pulling rate (m/s)	V_g	8×10^{-7}
Initial dimensionless concentration	$C = c / C_0$	1
Difference temperature (K)	$\Delta T = T_h - T_c$	10-10^3
Gradient temperature length (m)	L_g	0.138

TABLE II
Thermo Physical Property Data Used in Analysis [19]

Quantity	Symbol	Value
Density (kg/m^3)	ρ	5.5×10^3
Kinematic viscosity (m^2/s)	ν	1.3×10^{-7}
Thermal conductivity (W/^{0}C m)	λ	27.8
Specific heat (J/ $^\circ$C.Kg)	c_p	390
Thermal expansion coefficient of (C^{-1})	β_T	5×10^{-4}
Solutal expansion coefficient of (C^{-1})	β_S (mole fraction)$^{-1}$	-0.3
Diffusion coefficient (m^2/s)	D	1.3×10^{-8}
Partition coefficient	k_p	0.1
Latent heat (J/kg)	ΔH	460×10^3

For the cases without ampoule rotation, for $(0\le f_s\le0.2)$, the results at different convection levels $(10^3\le Gr\le10^5)$ are shown at $(t=20)$ in Fig. 2. In each plot, the left-hand side represents the concentration lines, while the right-hand side the stream function contours. For $(\Delta T=10)$, the convection in the melt $(f_s=0)$ is weak and the flow is monocellular. In this case, the dopants profile distribution is diffusive (see Fig. 2 (a)). In practice, is not real to have a temperature profile of $(\Delta T=10)$. However, have a diffusive mass transfer is a perfect condition.

In the second case, as the buoyancy force is considered, at $(\Delta T=10^3)$, a cellular flow upon the growth front is induced due to radial thermal gradients. Although the flow intensity is low, the local dopant field near the mushy zone is affected significantly which can be seen from the distortion of the iso-concentration lines (see Fig. 2 (b)). As a result, the radial dopant segregation increases (Fig. 3).

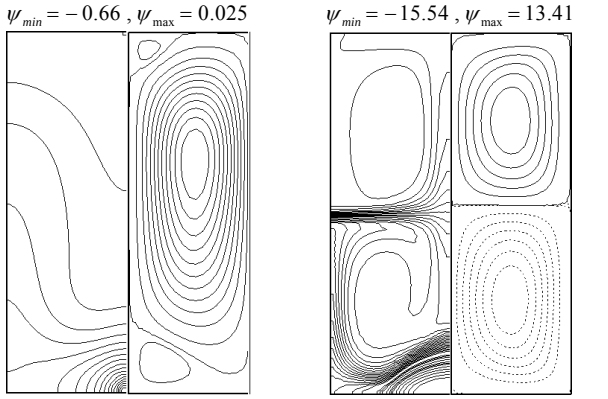

Fig. 2 Calculated flow patterns and dopant field

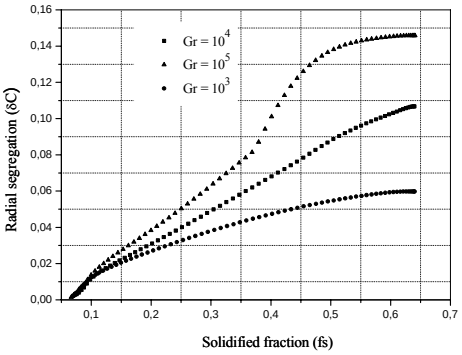

Fig. 3 Effect of buoyancy convection level on radial segregation during solidification

With ampoule rotation case, which the flow generated by the Coriolis force is proportional to (Re^{-1}), the unsteady state results at $\mathrm{Re}=0.1$ and $\mathrm{Re}=10$ are shown in Fig. 4. The effect of Reynolds number Re is illustrated in Figs. 4-5 for $Gr=3.6\times10^5$ where the buoyancy convection is well pronounced at the interface.

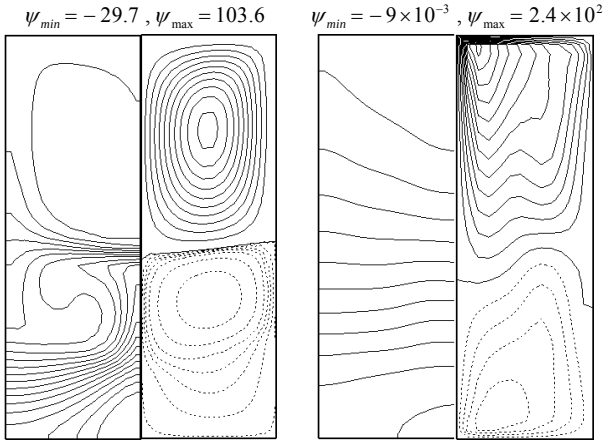

Fig. 4 Calculated flow patterns and dopant fields for: (a) Re = 0.1 , (b) Re = 10

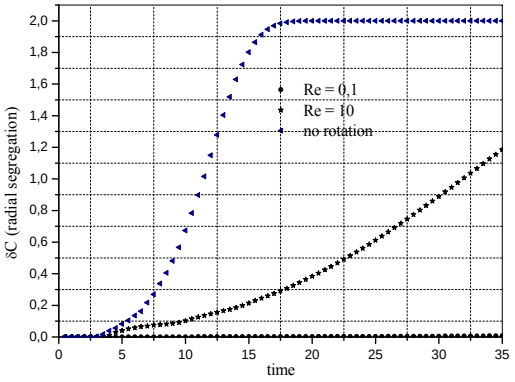

Fig. 5 Effect of rotation rate on radial segregation during solidification

At $\mathrm{Re} = 0.1$, the flow generated by the ampoule rotation becomes very important in the mushy zone $(0 \prec fs \prec 1)$ (see Fig. 4 (a)). It will induce the redistribution of solute at the interface. More importantly, the rotation moves the flow cell toward the ampoule wall and stretches it axially. As shown, the main flow cell fills almost the whole melt domain. As result, the elongated cell brings dopant mixing deeply into the bulk melt. Therefore the radial dopant segregation decreases due to poorer local mixing near the growth front. This will mean that, the suppression of the natural convection at the interface by ampoule rotation is effective when the convection level is high. The radial dopant segregation is also greatly reduced (Fig. 5).

Although the flow becomes low in liquid and mushy zones at $\mathrm{Re} = 10$, but the flow generated by ampoule rotation was not sufficient to more reduce the chemical segregations. In order that rotation has a positive effect on reducing chemical segregation, the flow generated by the ampoule rotation must be greater than that generated by the temperature profile.

IV. Conclusion

The ampoule rotation effect on the flows and dopant segregation in vertical Bridgman crystal growth is investigated numerically. From the calculated results, it's clear that a moderate ampoule rotation speed can significantly affect the flows, solidification fraction and further the dopant mixing. Similar to axially magnetic damping, the Coriolis force due to ampoule rotation can suppress thermal convection. The flow inhibition by ampoule rotation can be regarded as an extension of the Taylor-Proudman theorem for inviscid melt. In summary, ampoule rotation is believed to have large effects on vertical Bridgman crystal growth. However, how to better control the melt convection and dopant transport by ampoule rotation still requires further study, mainly, through crystal growth experiments.

Acknowledgments

The authors acknowledge financial support provided by the Unity of development and technology of Silicon (Algiers, Algeria) for the experimental data and Houari Boumedienne University (USTHB).

References

[1] Gault A, Monberg E, Clemans J(1986), J. Crystal Growth 74: 4-491.
[2] Hoshikawa K, Nakanishi H, Kohda H, Sasaura M (1989), J. Crystal Growth 94: 635-643.
[3] Monberg E, Gault W, Simchock F, Domingguez F (1987), J. Crystal Growth 83:160-174.
[4] Jun L, Bofeng B (2008), J. Crystal Growth 311: 20 -38.
[5] Mitric A, Duffar Th (2008), J. Crystal Growth 310:1490 -1511.
[6] Lia X, Rena Z, Fautrelleb Y (2006), J. Crystal Growth 290 : 571-590
[7] Henrya D, Ben Hadida H, Kaddecheb S, W(2008), J. Crystal Growth 310 -1533.
[8] Nouri S, Benzeghiba M, Benzaoui A(2011) Numerical study of the vertical solidification proce. Energy Procedia 6: 531-540.
[9] Jun L, Bofeng B, J(2008). Crystal Growth 311 -38.
[10] Liua Y, Yub W, Rouxc B, Lyubimovad T, Lana C(2006), Chemical Engineering Science 61-7766.
[11] Liua Y, Yub W, Rouxc B, Lyubimovad T, Lana C(2009), J. Crystal Growth 311 – 684.
[12] Zhang Y , Liu a, Jiang W, Pan X, Jina W, Ai F(2008) Segregation control of vertical Bridgman growth of Ga-doped germanium crystals by accelerated crucible rotation: ACRT versus angular vibration. J. Crystal Growth 311: 310 -5432.
[13] Capper P, Maxey C, Butler C, Grist M, J. Price(2005) Bulk growth of cadmium mercury telluride (CMT) using the Bridgman/accelerated crucible rotation technique (ACRT). J. Crystal Growth 275: 259- 275.
[14] Liu Y, Roux B,. Lan C(2007), Effects of accelerated crucible rotation on segregation and interface morphology for vertical Bridgman crystal growth: Visualization and simulation. J. Crystal Growth 304: 236-243.
[15] Lan C, Liang M, Chian J(2006) , Phase field modeling of convective and morphological instability during directional solidification of an alloy J. Crystal Growth 295: 212 -340.
[16] Voller V and Prakash K(1987) A fixed grid numerical modeling methodology for convection-diffusion mushy region phase-change problems. Int. J. Heat Mass Transfer 30:1709-1719.
[17] Carman P(1937), Tran.inst.Chem. engrs 15: 150-166.
[18] Timchenko V, Chen P, Leonardi E, de Vahl Davis G, Abbaschian R (2000) Int.J.Heat Mass Transfer 43: 963-980.
[19] Nouri S, Benzeghiba M, Benzaoui A(2011), Numerical Analysis of Solute Segregation in Directional Solidification under Static Magnetic Field, Defect and Diffusion Forum 312: 253-258.